Electronic Supplementary Material (ESI) for Nanoscale Horizons.

Supporting Information

Evidence of a Magnetic Transition in Atomically Thin $Cr_2TiC_2T_x$ MXene

Kanit Hantanasirisakul[1,2], Babak Anasori[1,2,⊥,*], Slavomir Nemsak[3], James, L. Hart[2,†], Jiabin Wu[1,2,4], Yizhou Yang[2], Rajesh V. Chopdekar[3], Padraic Shafer[3], Andrew F. May[5], Eun Ju Moon[2], Jun Zhou[4], Qinghua Zhang[6], Mitra L. Taheri[2,†], Steven J. May[2] & Yury Gogotsi[1,2,*]

[1]A.J. Drexel Nanomaterials Institute, Drexel University, Philadelphia PA 19104, United States

[2]Department of Materials Science and Engineering, Drexel University, Philadelphia, PA 19104, United States

[3]Advanced Light Source, Lawrence Berkeley National Laboratory, Berkeley, CA 94720, United States

[4]Wuhan National Laboratory for Optoelectronics, Huazhong University of Science and Technology Wuhan 430074, Hubei, P. R. China

[5]Materials Science and Technology Division, Oak Ridge National Laboratory, Oak Ridge, TN 37831, United States

[6]Beijing National Laboratory for Condensed Matter Physics and Institute of Physics, Chinese Academy of Sciences, Beijing 100190, P. R. China

[⊥] current address: Mechanical and Energy Engineering, Integrated Nanosystems Development Institute, Purdue School of Engineering and Technology, Indiana University-Purdue University Indianapolis, IN 46202, United States

†current address: Department of Materials Science and Engineering, Johns Hopkins University, Baltimore, MD 21218, United States

[*]Corresponding author: Yury Gogotsi (gogotsi@drexel.edu), Babak Anasori (banasori@iupui.edu)

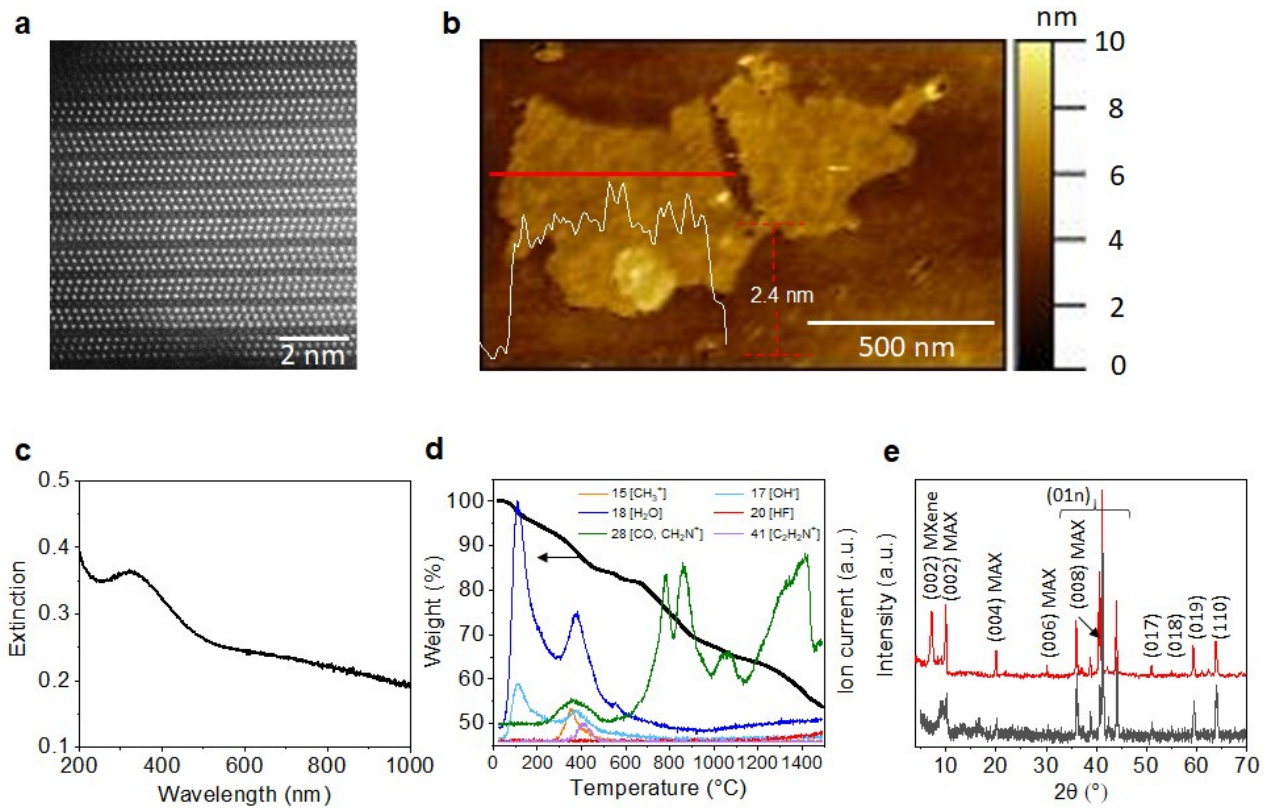

Figure S1. Characterization of Cr_2TiAlC_2 MAX and $Cr_2TiC_2T_x$ MXene. a) Cross-section transmission electron micrograph of Cr_2TiAlC_2 MAX phase. b) Atomic force microscopy image of 2D $Cr_2TiC_2T_x$ flake. Inset shows a line profile across the red line. c) UV-visible-NIR spectrum of d-$Cr_2TiC_2T_x$ solution conducted using a spectrometer (Evolution 201, Thermo Scientific), scanning from 200 to 1,000 nm and normalized at 264 nm. DI water was used as a blank. d) TGA-MS analysis of $Cr_2TiC_2T_x$ free-standing film. e) XRD patterns of Cr_2TiAlC_2 MAX phase (gray) and multilayered $Cr_2TiC_2T_x$ (red).

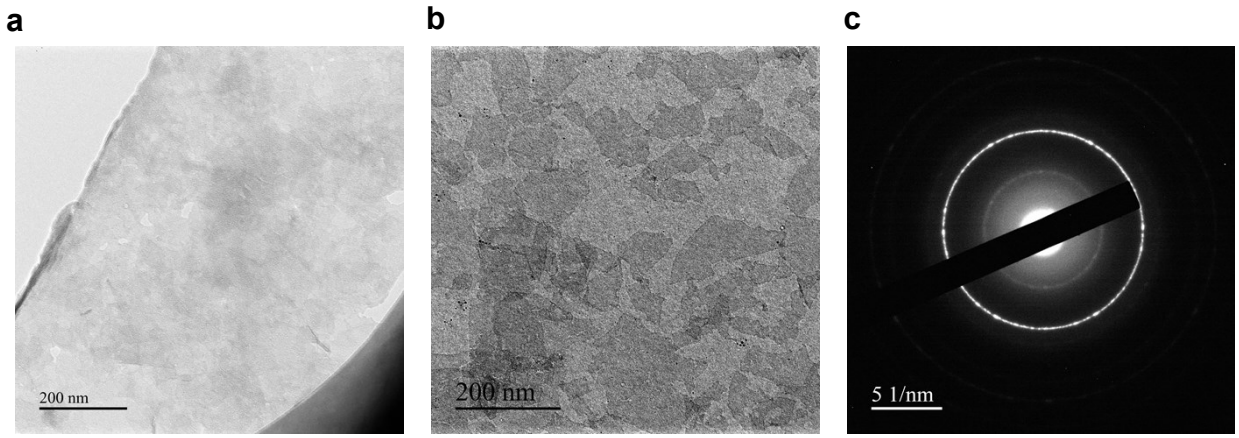

Figure S2. TEM and electron diffraction analysis. a-b) Plane-view transmission electron micrographs of $Cr_2TiC_2T_x$ after annealing at 400 °C over a large area (~0.5 μm^2). Negligible secondary phase was observed in both images. c) Selected-area electron diffraction of the same sample after annealing at 700 °C. The first ring of intensity is assigned to (-110), and the second to (110), consistent with multiple MXene flakes with their *c*-axis parallel to the beam. The diffuse intensity at low scattering angels is attributed to the amorphous SiN support film, which the MXenes are supported on. No other crystalline impurity was observed in the SAED pattern. The annealing was done inside a TEM column with a baseline pressure of 10^{-5} Pa.

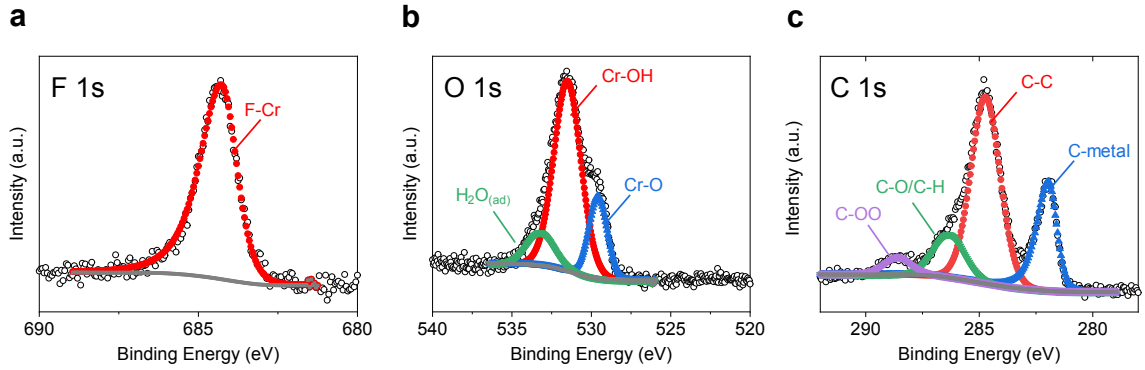

Figure S3. XPS analysis of $Cr_2TiC_2T_x$ free-standing film. Core level XPS spectra of **(a)** F 1*s*, **(b)** O 1*s*, and **(c)** C 1*s* regions.

Table S1. Summary of XPS analysis

Region	Binding Energy (eV)	Full Width at Half Maximum (eV)	Assignment	Atomic Concentration (%)
Cr $2p_{3/2}$	574.8	2.0	Cr-C	7.08
	576.8	2.8	Cr-T_x	3.32
Ti $2p_{3/2}$ ($2p_{1/2}$)	455.0 (461.1)	0.6 (1.3)	Ti-C	1.58 (0.79)
	455.6 (461.0)	1.6 (2.1)	Ti (II)	2.53 (1.26)
	458.5 (464.1)	2.2 (3.3)	Ti (IV)	1.06 (0.53)
F 1*s*	684.3	1.1	F-Cr	8.88
O 1*s*	529.6	1.4	O-Cr	4.76
	531.5	1.9	HO-Cr, O-C	16.24
	533.2	1.9	$H_2O_{(ad)}$	2.77
C 1*s*	281.9	0.9	C-metal	12.31
	284.7	1.5	C-C	27.73
	286.3	1.6	C-O/C-H	6.76
	288.6	1.4	C-OO	2.39

From the table, the deduced atomic concentration is Cr:Ti:C:F:O:OH (C-O) = 1.7:1:1.99:1.44: 0.77: 2.6. The atomic concentration was normalized by taking Ti concentration equal to 1. Because the binding energy of Cr-OH bonds overlaps with C-O bonds that typically exist on MXene film surface, the precise amount of -OH termination cannot be determined.

Table S2. Atomic concentration deduced from energy dispersive X-ray spectroscopy (EDX) of the as-synthesized film and the film annealed at 500 °C under Ar.

	As-synthesized		500 °C, Ar	
	Atomic concentration (%)	Normalized atomic concentration	Atomic concentration (%)	Normalized atomic concentration
Cr	16.93 ± 0.34	2.09 ± 0.04	21.15 ± 0.94	2.09 ± 0.09
Ti	8.06 ± 0.17	1.00 ± 0.00	10.11 ± 0.15	1.00 ± 0.00
F	12.13 ± 0.12	1.50 ± 0.01	9.14 ± 0.63	0.90 ± 0.06
O	36.66 ± 0.58	4.52 ± 0.07	35.15 ± 0.41	3.48 ± 0.04
C	26.23 ± 0.67	3.23 ± 0.08	24.46 ± 0.09	2.42 ± 0.01

Note that EDX is not sensitive to chemical environment of the elements. Therefore, the atomic concentration of O and C also includes other species than $Cr_2TiC_2T_x$. The normalized atomic concentration of Cr, Ti, and F is calculated based on the assumption that the free-standing film samples only contain atomically thin $Cr_2TiC_2T_x$, and the atomic concentration of Ti is set to 1.

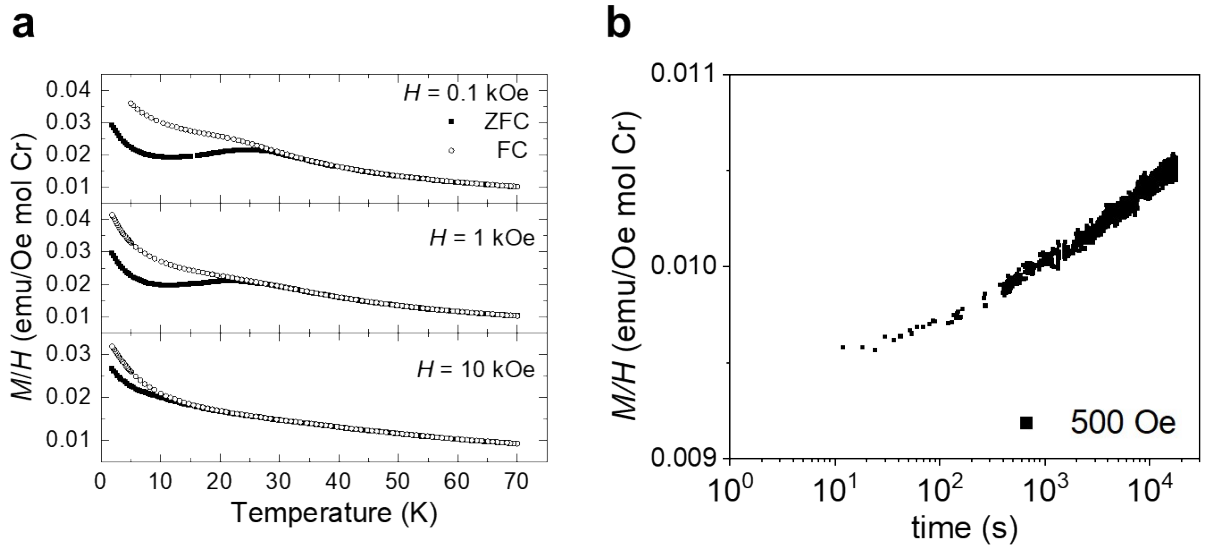

Figure S4. a) Zero-field-cooled (filled squares) and field-cooled (empty circles) dc magnetization of $Cr_2TiC_2T_x$ MXene measured from 2-70 K with magnetic field ranges from 0.1 to 10 kOe. b) Time-dependent magnetization measured at 10 K in a 500 Oe magnetic field. For this measurement, the sample was cooled without a field from room temperature to 10 K, and it was held at this temperature for a wait time (t_w) of 100 s before applying the field.

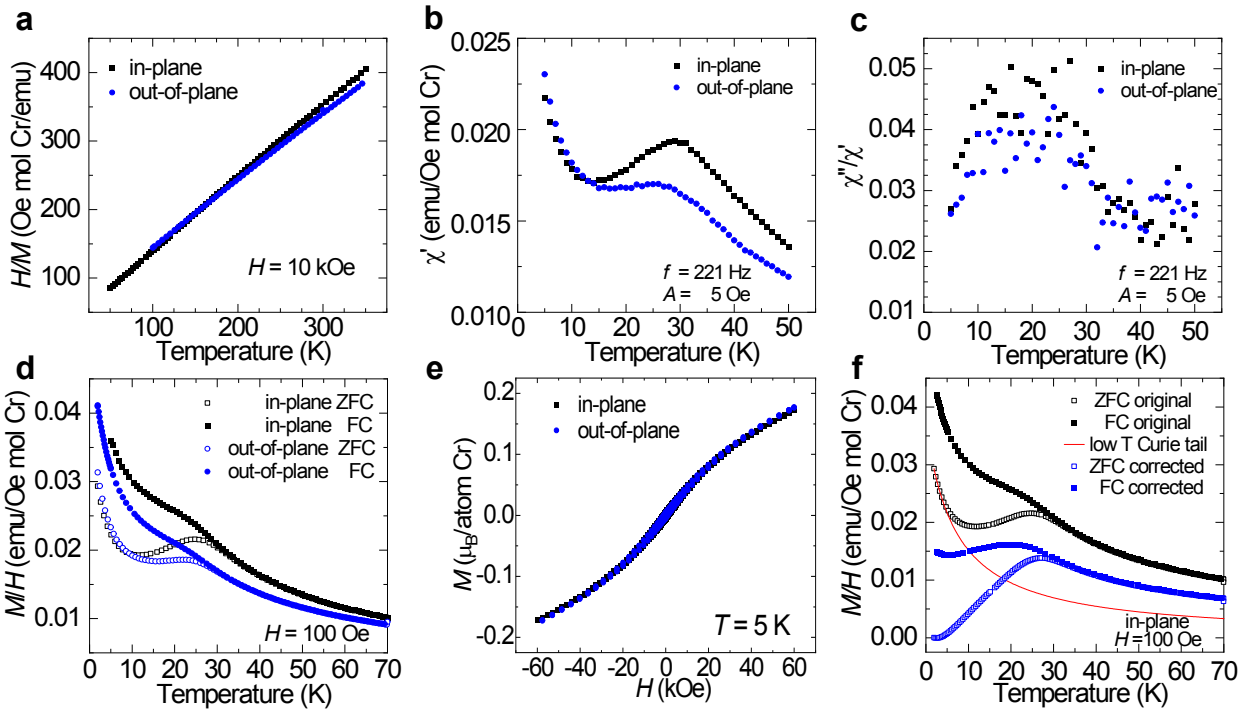

Figure S5. Anisotropy in magnetization measurements. a) 1/(*M*/*H*) above T_f, b) in-phase component of the ac susceptibility, c) ratio of the out-of-phase to in-phase component of the ac susceptibility, and d) dc magnetization as a function of temperature around T_f. The freezing temperature appears to be slightly lower when the field is applied out-of-plane. e) Isothermal magnetization as a function of field at 5 K. f) Measured ZFC-FC magnetization (black) with the thin red line showing a Curie-Weiss fit to the low-temperature magnetization to account for the so-called Curie tail from paramagnetic spins. The blue data show the magnetization after subtraction of this low-temperature paramagnetic contribution, revealing magnetization consistent with glassy behavior.

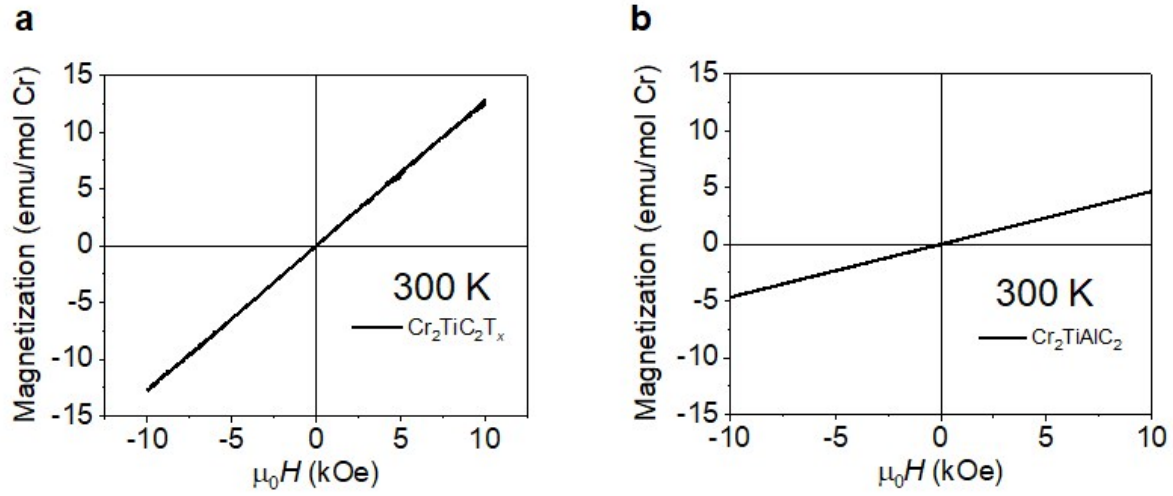

Figure S6. Field-dependent magnetization of a) $Cr_2TiC_2T_x$ free-standing film and b) Cr_2TiAlC_2 MAX powder measured at 300 K. The linear dependence observed is typical for paramagnets.

We repeated the ZFC-FC measurements on several $Cr_2TiC_2T_x$ free-standing films dried either at room temperature (RT), 150 °C, or 500 °C as well as multilayered (ML) powders and found that the cusp in the ZFC curve is always present within the temperature range from 22 to 40 K. The batch-dependent variation in the transition temperature might be due to different surface terminations of different samples.

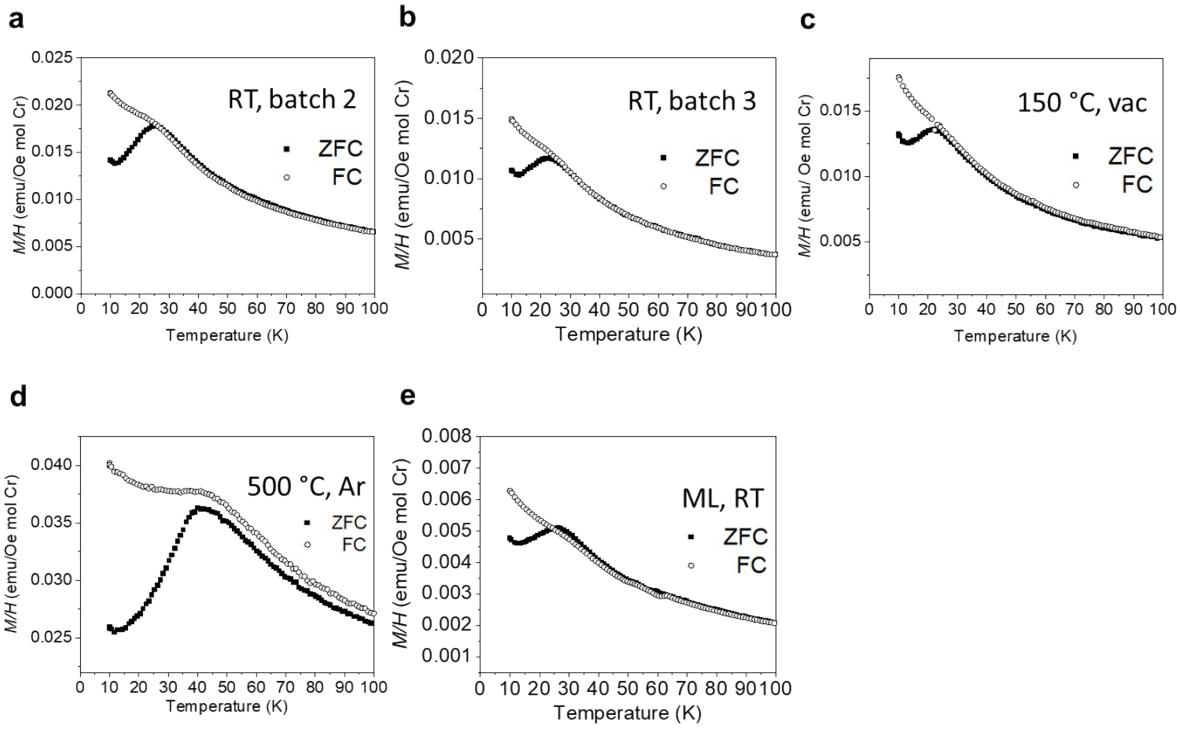

Figure S7. Reproducibility of magnetic measurements. Zero-field-cooled (ZFC) and field-cooled (FC) magnetization measured with 500 Oe magnetic field of two different batches of $Cr_2TiC_2T_x$ free-standing film dried at room temperature (a) and (b), (c) $Cr_2TiC_2T_x$ free-standing film dried at 150 °C under vacuum, (d) $Cr_2TiC_2T_x$ free-standing film dried at 500 °C under Ar, and (e) multilayered (ML) particles dried at room temperature. The magnitude of magnetization for the multilayer sample is much smaller than that of the free-standing film sample because it contains some amount of unetched MAX particles, which show smaller magnetization as shown in Figure 2 and 3 of the main text.

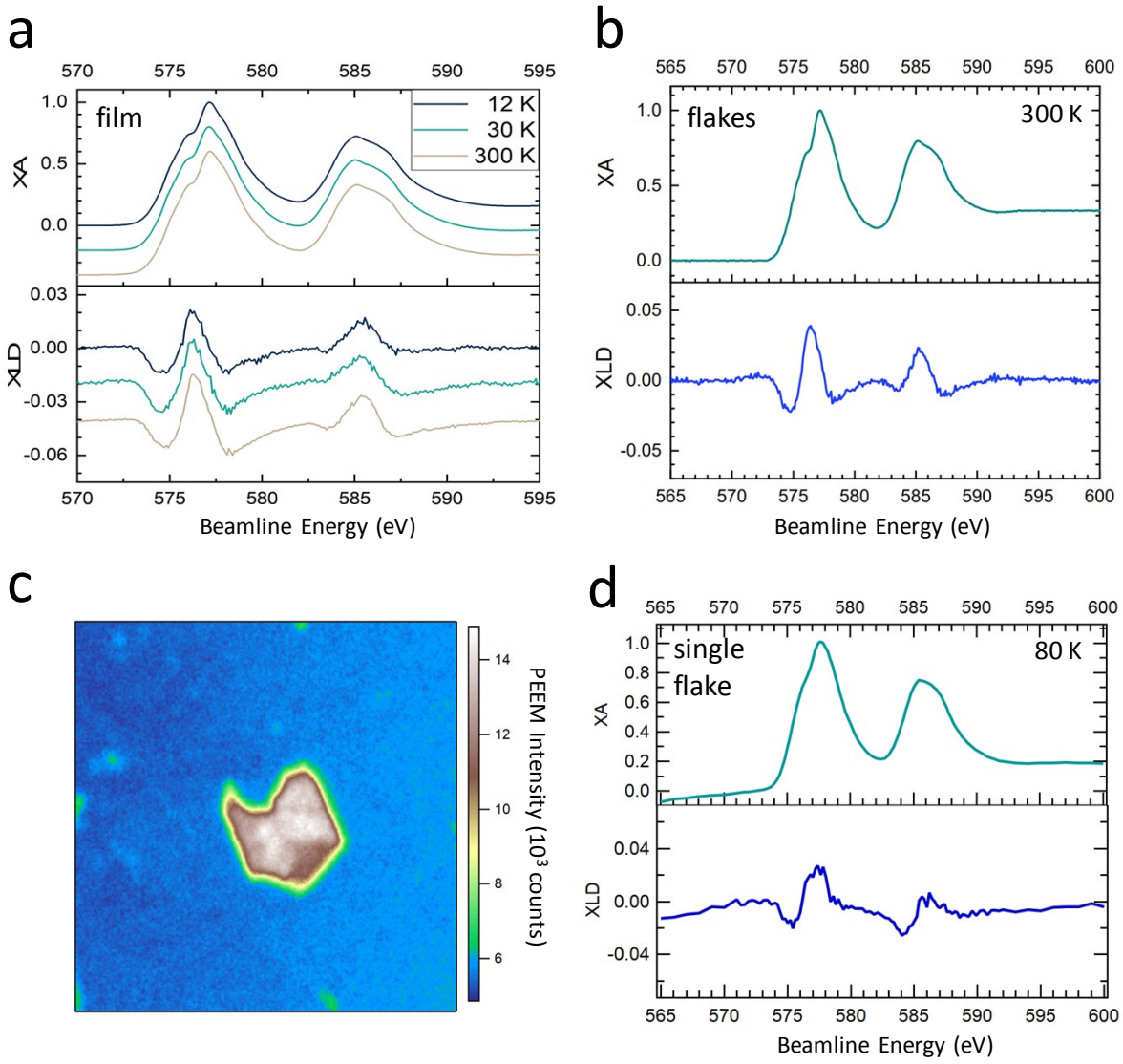

Figure S8. X-ray absorption spectroscopy. a) Temperature series of X-ray absorption (XA) spectra and X-ray linear dichroism (XLD) signal of $Cr_2TiC_2T_x$ free-standing paper collected over the Cr *L*-edge. b) XA and XLD measurement of the $Cr_2TiC_2T_x$ flakes dispersed on doped Si substrate, averaged over 100 ×100 μm^2 area. c) PEEM micrograph of the individual flake integrated over L_3 absorption edge maximum (photon energies 577.2-578.0 eV). d) XA and XLD of a single flake from panel c).

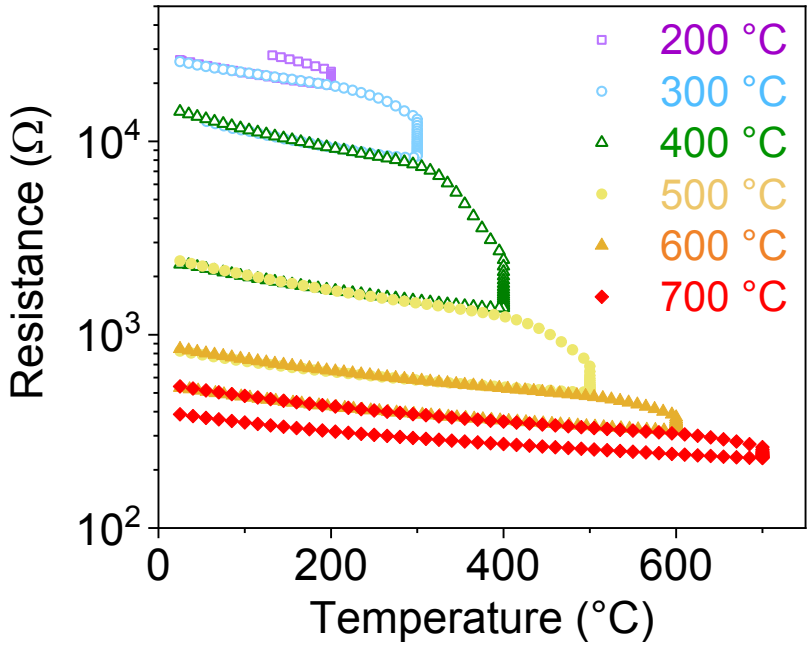

Figure S9. Temperature-dependence of resistance measured during in situ annealing in vacuum. The room temperature resistance decreased by approximately two orders of magnitude from the pristine state (purple) throughout annealing cycles up to 700 °C (red), after which the sample degraded as correlated with thermogravimetric-mass spectroscopy analysis (TGA-MS) (Figure S1d). The decrease in the resistance during the 200 °C and 300 °C annealing steps corresponds to the desorption of intercalated water molecules at ~115 °C and from 300 °C, while a larger decrease of resistance during the 400 °C and 500 °C annealing steps corresponds to decomposition of tetramethylammonium hydroxide (TMAOH) molecules, in good agreement with TGA-MS results. Interestingly, unlike other MXenes, the slope of the *R vs T* (d*R*/d*T*) remains negative after removal of the intercalants, suggesting that the negative d*R*/d*T* observed during the in situ annealing experiment may be the intrinsic semiconducting nature of this $Cr_2TiC_2T_x$ MXene. These measurements were performed using DENS solutions Lighting D9+ sample holder A1 heating/biasing nanochips. d-$Cr_2TiC_2T_x$ solution was drop-casted onto the chip and dried in air. Resistance values were obtained using a 4-point geometry with a Keithley 2400 SMU. Annealing steps were performed with 100 °C intervals from 200 to 700 °C. Heating/cooling rates were set to 1 °C/s. For each annealing step, the maximum temperature was held for 5 min. The annealing was done inside a TEM column with a baseline pressure of 10^{-5} Pa.

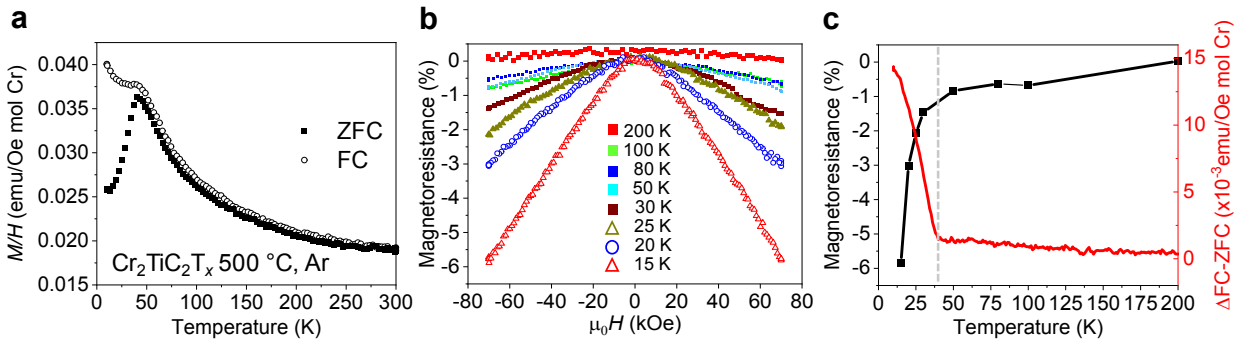

Figure S10. Magnetic and magnetoresistance characterization of $Cr_2TiC_2T_x$ free-standing film annealed at 500 °C under Ar. a) Zero-field-cooled (filled squares) and field-cooled (empty circles) magnetization from 10-300 K measured with 500 Oe magnetic field. b) Field-dependent magnetoresistance measured from 15 to 200 K. c) A comparison between magnitude of magnetoresistance measured at 70 kOe (left axis) and the difference between the field-cooled and zero-field-cooled magnetization (right axis).

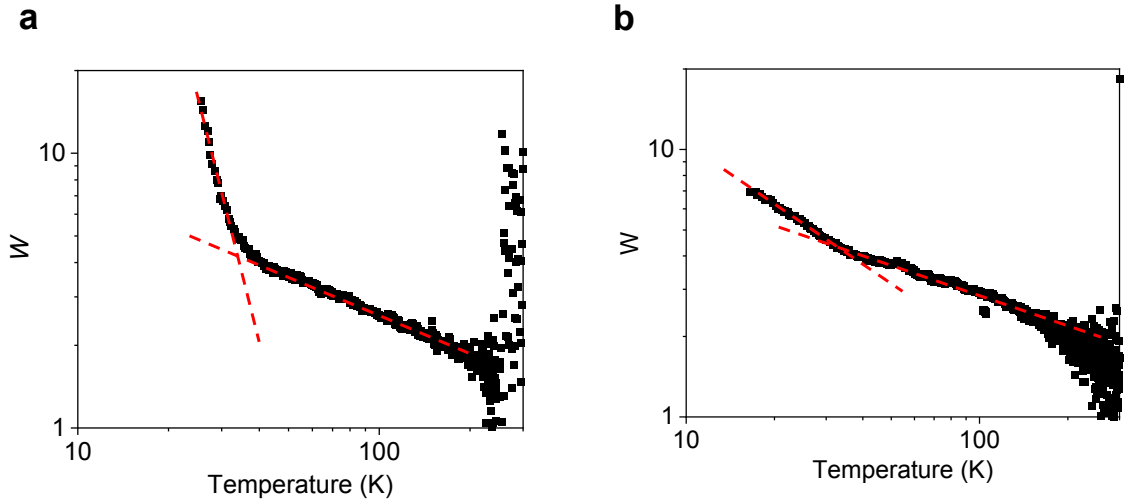

Figure S11. Reduced activation energy (W) calculated from $W(T) = -\,d \ln \rho(T)/\, d \ln T$. Panels a) and b) show the log-log plot of reduced activation energy (W) with temperature for two different $Cr_2TiC_2T_x$ free-standing films. Both data show an inflection point at around 30 K. Both samples were annealed at 150 °C.

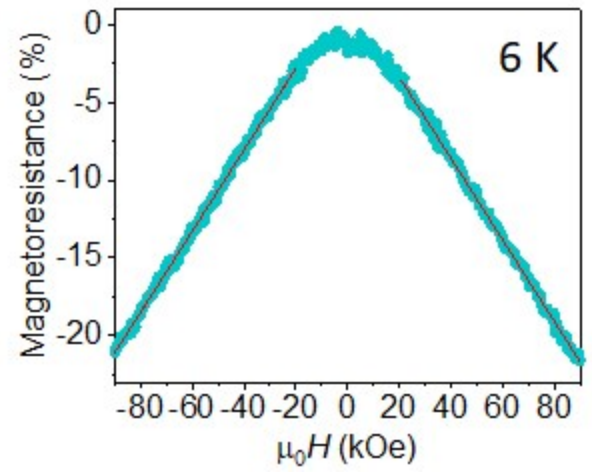

Figure S12. Field-dependent magnetoresistance of $Cr_2TiC_2T_x$ free-standing film annealed at 150 °C measured at 6 K. The data at both negative and positive fields was fitted from ±20 to ±90 kOe with a linear equation MR = $\pm 2.61\times10^{-4}H+2.93$ with $R^2 > 0.998$.

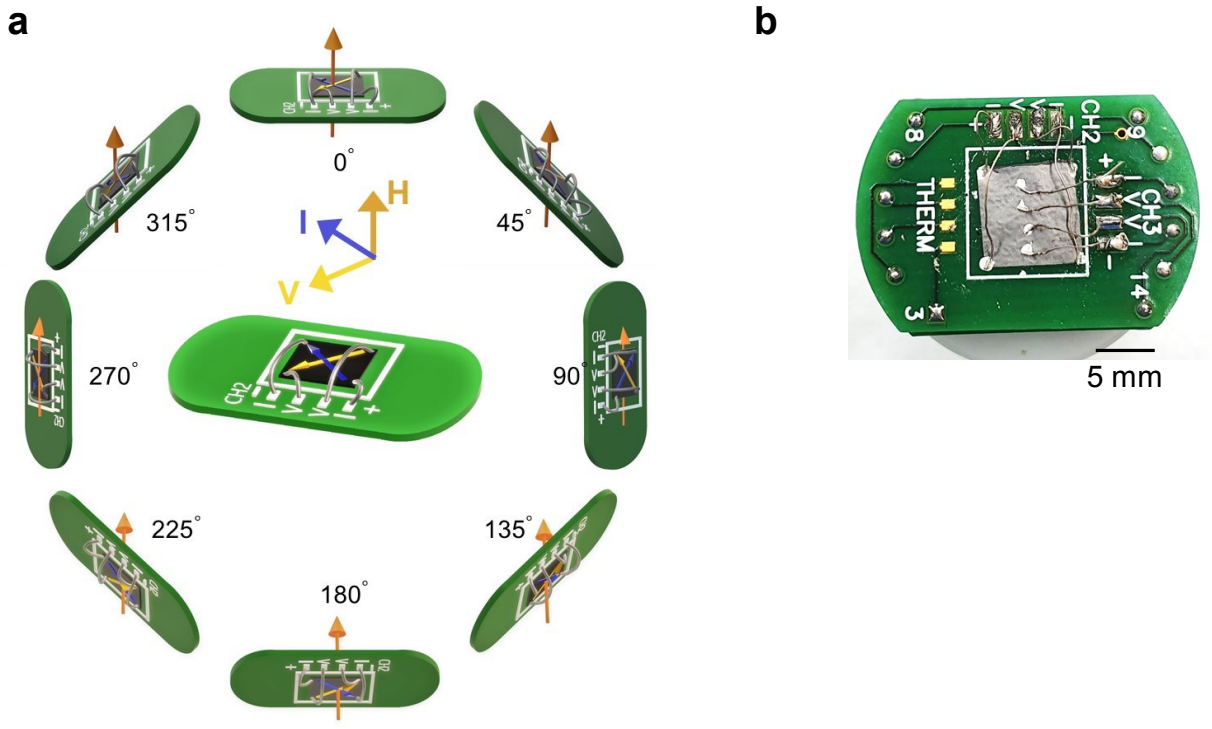

Figure S13. a) The direction of the applied magnetic field (*H*) in relation to the sample, applied current (*I*) and measured voltage (*V*) during the AMR measurements. b) Optical image of the sample holder for angle-dependent magnetoresistance (AMR) measurements. MXene free-standing films were wired in 4-point geometry and van der Pauw configurations.

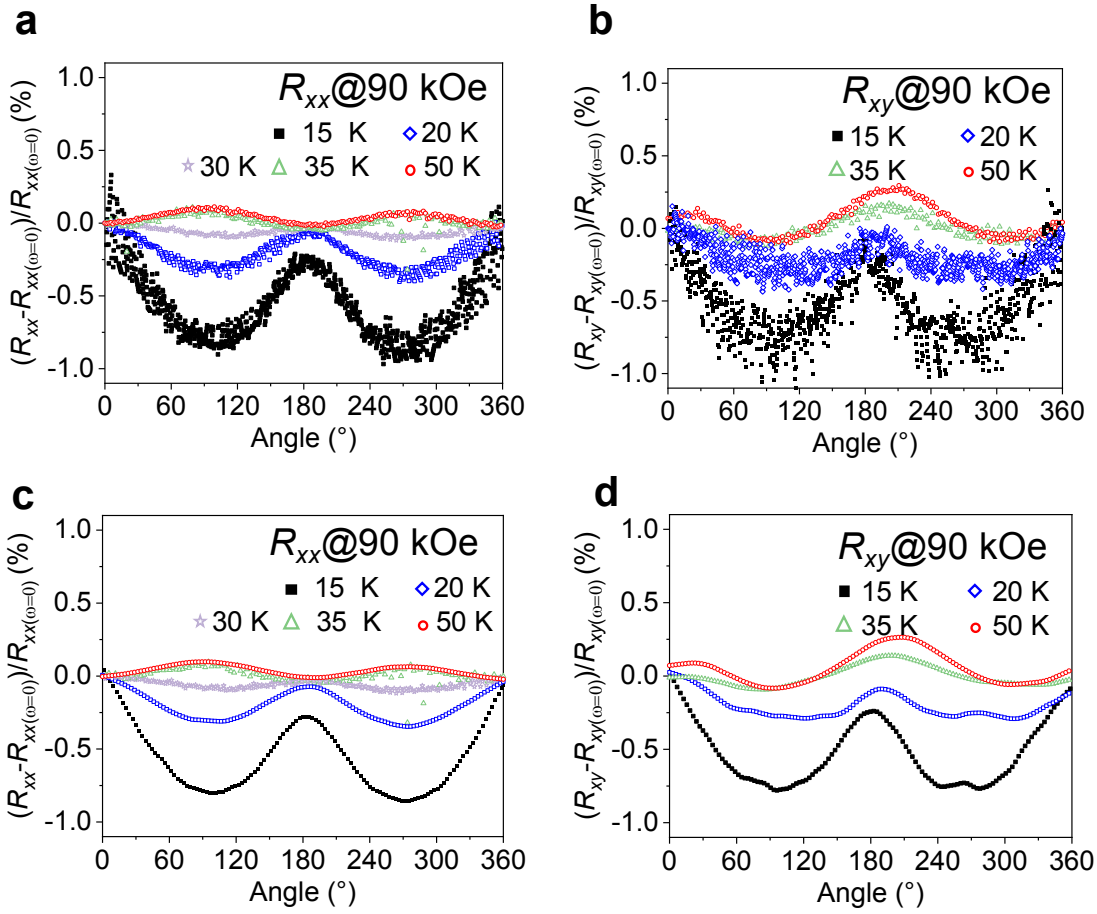

Figure S14. Raw data of (a) normalized angular-dependent magnetoresistance (R_{xx}) and (b) normalized angular-dependent Hall resistance (R_{xy}) measured at 90 kOe from 15 to 50 K for $Cr_2TiC_2T_x$. The smoothed data of (a) and (b) are shown on panels (c) and (d), respectively.

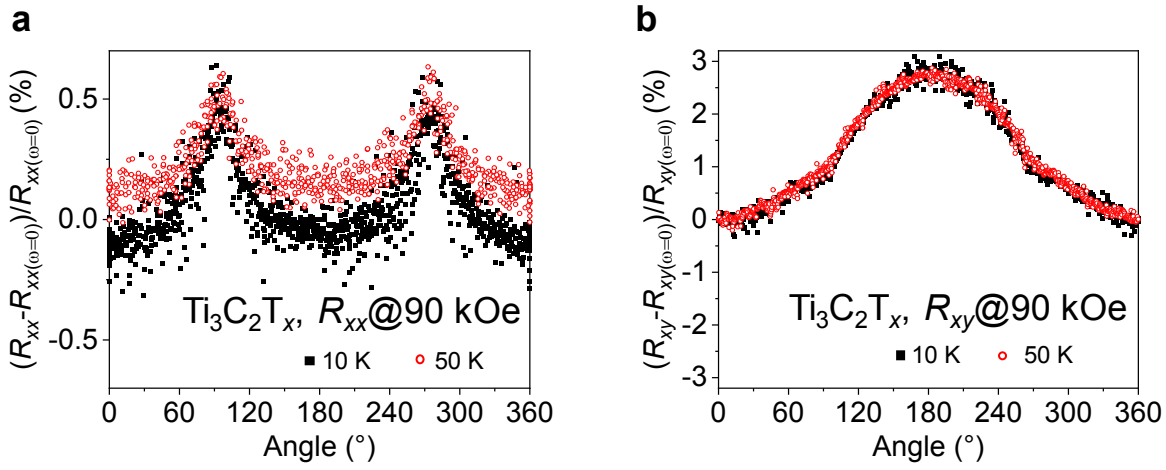

Figure S15. AMR of $Ti_3C_2T_x$ free-standing film. a) Normalized angular-dependent magnetoresistance (R_{xx}) and b) normalized angular-dependent Hall resistance (R_{xy}) measured at 10 and 50 K with 90 kOe magnetic field.